Liposomal oxygen-generating hydrogel for enhancing cell survival under hypoxia condition

Saeid Moghassemi[1,*], Arezoo Dadashzadeh[1,*], Hafez Jafari[2], Pejman Ghaffari-Bohlouli[2], Amin Shavandi[2], Christiani A. Amorim[1,**]

[1] Pôle de Recherche en Physiopathologie de la Reproduction, Institut de Recherche Expérimentale et Clinique, Université Catholique de Louvain, Brussels, Belgium

[2] BioMatter unit - École polytechnique de Bruxelles, Université Libre de Bruxelles, Avenue F.D. Roosevelt, 50 - CP 165/61, 1050 Brussels, Belgium

*These authors contributed equally to this work

** Corresponding author: Prof. Christiani Amorim
Pôle de Recherche en Physiopathologie de la Reproduction
Institut de Recherche Expérimentale et Clinique, Université Catholique de Louvain
Avenue Hippocrate 55, bte B1.55.03, 1200 Brussels, Belgium
E-mail: christiani.amorim@uclouvain.be
Tel: +32 (0)2 43 61017

Number of words: 8421
Number of tables: 1
Number of figures: 7

25 ***Graphical Abstract***

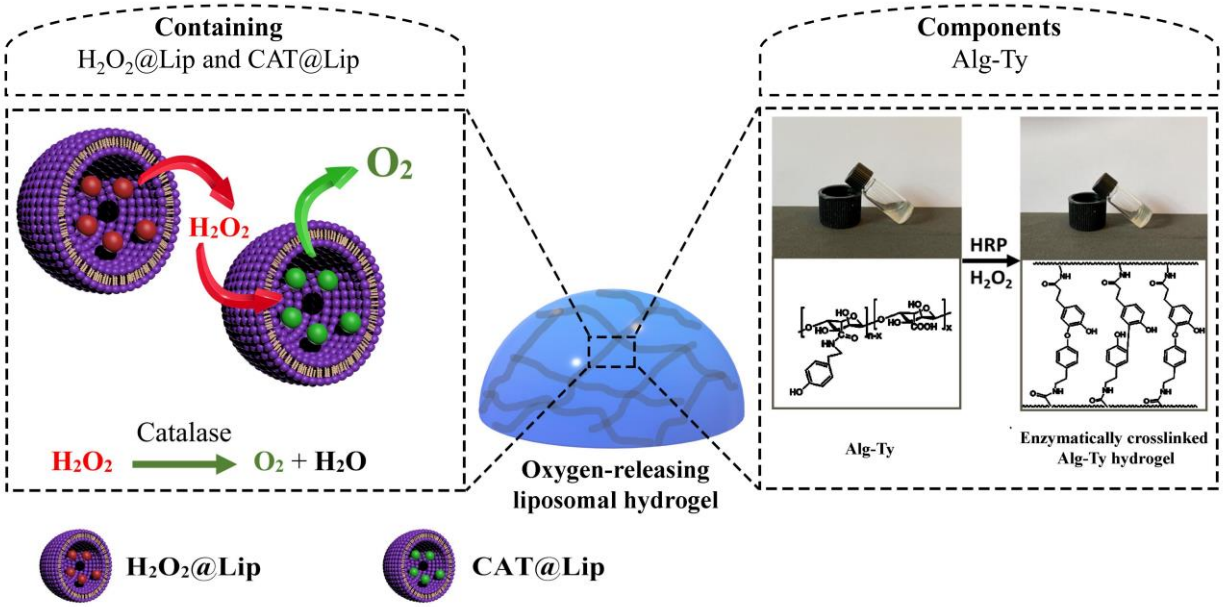

26

27

Abstract

The inadequate oxygen supply to engineered tissues has been a persistent challenge in tissue engineering and regenerative medicine. To overcome this limitation, we developed a scaffold combined with an oxygen-releasing liposomal system comprising catalase-loaded liposomes (CAT@Lip) and H_2O_2-loaded liposomes (H_2O_2@Lip). This oxygenation system has shown high cytocompatibility when they were applied to human stromal cells. Under hypoxic conditions, the cell viability enclosed in the oxygen-releasing liposomal alginate hydrogel (94.62 ± 3.46 %) was significantly higher than that of cells enclosed in hydrogel without liposomes (47.18 ± 9.68 %). There was no significant difference in cell viability and apoptosis rate compared to normoxia conditions after three days, indicating the effectiveness of the oxygen-releasing approach in hypoxic conditions. In conclusion, our study demonstrates that the use of liposomal oxygen-releasing scaffolds can overcome the oxygen diffusion challenge in tissue implant fabrication, providing a simple solution for cellular oxygenation that could be a crucial element in tissue engineering.

Keywords

Tissue engineering; Oxygen-releasing; Liposome; Hydrogel; Alginate

1 Introduction

Tissue engineering strategies have made significant progress in protecting, restoring, or improving the functionality of injured organs or tissues. However, one of the persistent challenges is the supply of oxygen and nutrients to the encapsulated cells in scaffolds [1]. The host vascular system supplies oxygen and essential nutrients in the original tissue, thereby facilitating cell survival and proliferation. The original tissue receives oxygen and essential nutrients from the host vascular system, facilitating cell survival and proliferation. The development of vascularization in tissue constructs is a gradual process, and the prolonged duration can lead to a significant amount of cellular death. To overcome the effects of hypoxia, considerable efforts have been made to provide adequate levels of essential nutrients and oxygen to the affected areas. Oxygen-releasing biomaterials are among the most promising strategies to overcome oxygen diffusion limitations in tissue constructs [2, 3]. These biomaterials provide the cells with the necessary oxygen supply for their survival and metabolic function until optimum vascularization is achieved [4]. One of the most interesting strategies to provide oxygen in biomaterials is based on the decomposition of hydrogen peroxide (H_2O_2) into water and oxygen, which can be accelerated by catalase [5]. Therefore, some groups have explored the feasibility of using H_2O_2 for oxygenation within biomaterials. For example, Abdi et al. [6, 7] employed a double emulsion/solvent evaporation technique to fabricate H_2O_2-loaded PLGA particles, enhancing the vitality of muscle cells during tissue regeneration. Additionally, this approach holds promise for boosting oxygen levels in cancer therapy. Similarly, Li et al. [8] established a methodology for producing core-shell oxygen-releasing microspheres, thus enhancing the viability of cardio-sphere-derived cells in hypoxic environments. The oxygen-delivering hydrogel exhibited substantial improvements

69 not only in cell viability but also the cells' differentiation capability. Recently, Song et al. [9,
70 10] investigated the potential of using liposomes to encapsulate either catalase or hydrogen
71 peroxide (H_2O_2) separately as a method to alleviate tumor hypoxia and enhance cancer radio-
72 immunotherapy. Catalase enzymes can decompose H_2O_2 into oxygen. Cationic liposomes
73 containing catalase have been reported to be effective in reducing the damage to alveolar
74 cells caused by hydrogen peroxide [11]. H_2O_2, being a polar molecule, slowly passes through
75 the lipid bilayer of liposomes, acting as the "fuel" for catalase-loaded liposomes (CAT@Lip)
76 to produce oxygen [12, 13]. Although it has shown promising results for
77 radioimmunotherapy, the impact of oxygenation on encapsulated cells in a tissue engineering
78 scaffold has not been studied yet.

79 The use of horseradish peroxidase (HRP)-mediated crosslinking is a promising approach for
80 developing *in situ* forming hydrogel with controllable gelation time and mechanical
81 properties for cell encapsulation [14, 15]. Natural and synthetic polymers such as alginate,
82 cellulose, and poly(ethylene glycol) can be modified with phenol-containing compounds like
83 tyramine to create phenol-functionalized polymer chains that can rapidly gel in the presence
84 of HRP and H_2O_2 via radical polymerization of tyramine residues [16, 17]. Moreover, when
85 used at concentrations of 2.5 U/mL and 10 mM, respectively, HRP and H_2O_2 had no adverse
86 effects on the viability of encapsulated human mesenchymal stem cells, indicating the
87 feasibility of this enzyme-mediated method for constructing cell-laden hydrogels [18].

88 Among natural polymers, alginate stands out due to its exceptional characteristics, including
89 biocompatibility, biodegradability, and ease of modification. The profusion of carboxylic acid
90 groups within the alginate structure renders it exceptionally amenable to the incorporation
91 of tyramine groups via carbodiimide coupling chemistry. This strategic incorporation

92 enables the fabrication of hydrogels characterized by customizable gelation durations and
93 mechanical attributes, accomplished through enzyme-mediated crosslinking mechanisms.

94 This study aims to investigate the impact of a liposomal oxygen-releasing hydrogel system
95 on the survival of human stromal cells in hypoxic conditions. For this purpose, we designed
96 and characterized catalase-loaded liposomes (CAT@Lip) and H_2O_2-loaded liposomes
97 (H_2O_2@Lip). These liposomal oxygen-releasing systems were incorporated into enzyme-
98 mediated crosslinked alginate hydrogels, along with isolated human ovarian stromal cells, to
99 evaluate their compatibility with cells. Finally, we assessed how our oxygenation strategy
100 influenced the viability and apoptosis rate of stromal cells under hypoxic conditions.

101

102

103 **2 Materials and Methods**

104 **2.1 Materials**

105 Sodium alginate (9005-38-3), 1-ethyl-3-(3dimethylaminopropyl)carbodiimide (EDC) (1892-
106 57-5; 98 %), N-hydroxysuccinimide (NHS) (6066-82-6; 98 %), horseradish peroxidase (HRP)
107 (P8375-1KU; Type VI, essentially salt-free, lyophilized powder, ≥250 units/mg solid), and
108 hydrogen peroxide (H_2O_2) (7722-84-1; 30 %), 1,2-Distearoyl-sn-glycero-3-phosphocholine
109 (P1138; DSPC), 1,2-Dioleoyl-sn-glycero-3-phosphoethanolamine (76548, DOPE), cholesterol
110 (C8667; CH), Liberase DH (05401089001), Triton X-100 (X100), 80 µm (NY8002500) and 30
111 µm (NY3002500) nylon net filters and trypan blue (T8154) were purchased from Sigma
112 Aldrich (Hoeilaart, Belgium). Dulbecco's modified Eagle's medium F-12 nutrient mixture
113 (21041-025, DMEM/F12), MEM/GlutaMAX™ (42360–024), heat-inactivated fetal bovine

114 serum (16140-071; HI FBS), antibiotics and antimycotic (15240-062; AA), Dulbecco's
115 Phosphate Buffered Saline with Ca^{2+} and Mg^{2+} (14040-091, DPBS) (1x), DNase (89836), and
116 trypsin/EDTA solution (0.2% of EDTA and 0.25% of trypsin in PBS (phosphate buffered
117 saline, 0.01 M pH 7.2), 25300) were obtained from Gibco Life Technologies Ltd. Tyramine
118 hydrochloride (60-19-5; >98 %) was obtained from Carbosynth (Carbosynth, Compton,
119 United Kingdom). Deuterium oxide (D_2O) was purchased from Eurisotop. PrestoBlue™ HS cell
120 viability reagent (P50200), LIVE/DEAD™ Viability/Cytotoxicity assay kit (L3224), 2',7'-
121 dichlorodihydrofluorescein diacetate (D399, DCFH-DA), normal goat serum (NGS), Amplex™
122 UltraRed reagent (A36006), and Alexa FluorTM 488 goat anti-rabbit IgG (A11034, Thermo
123 Scientific) were purchased from Thermo Fisher Scientific Corp. (Merelbeke, Belgium). Tween
124 20 (663684B), bovine serum albumin (3854.3; BSA), polyclonal anti-caspase-3 primary
125 antibody (9661S), and fluorescent mounting medium (S3023) were respectively purchased
126 from VWR (Radnor, AR, USA), Carl Roth (Karlsruhe, Germany), Cell Signaling Technology
127 (Beverly, MA, USA), and Dako (Glostrup, Denmark). All other chemicals were of the highest
128 grade commercially available.

129

130 2.2 Preparation of alginate-tyramine (Alg-Ty)

131 Alginate-tyramine (Alg-Ty) was prepared by conjugation of tyramine to the alginate
132 backbone chain via carbodiimide coupling chemistry [19]. Briefly, 0.5 g (3 mmol) EDC and
133 0.3 g (2.6 mol) NHS were added to a solution of 1 g of sodium alginate dissolved in 100 ml of
134 MES (2-(N-morpholino)ethane sulfonic acid) buffer (50 mM), and the pH was adjusted to 6
135 by 1 M NaOH. Then, 0.7 g (4 mmol) Tyramine hydrochloride was dissolved in 20 ml of MES
136 (50 mM) and added dropwise to the alginate solution, and continuously stirred for 24 h at

137 ambient temperature. The reaction mixture was dialyzed against (3500 Da cut off) distilled
138 water for three days, changing the water every 8 h. The final product was freeze-dried and
139 kept in a moisture-free desiccator before use. The conjugation of tyramine into the alginate
140 backbones was determined using ^{1}H NMR and ultraviolet-visible spectroscopy.
141

142 2.3 Preparation of CAT@Lip and H_2O_2@Lip

143 In this study, catalase-loaded liposomes (CAT@Lip) and H_2O_2-loaded liposomes (H_2O_2@Lip)
144 were prepared by the thin-film hydration method, followed by sonication [20]. Briefly, all
145 lipids, including DSPC, DOPE, and CH at the molar ratio of 1:1:1 were dissolved in 2 ml
146 chloroform and the solvent was evaporated for 30–35 min at 60°C. Then, the formed film was
147 purged using N_2 gas and dried using an overnight vacuum desiccator to remove any solvent
148 traces. After the film hydration by 1 mL of PBS solution containing 800mg/L catalase (CAT)
149 or 1 M H_2O_2, the mixture was vortexed, placed in an ultrasonic bath (Powersonic 405, 40 kHz)
150 at 40°C for 15 min, and subsequently, the suspension was centrifuged 20,000g for 20 minutes
151 at 4°C to separate the liposomes from the aqueous solution.

152 In the context of oxygen delivery applications, the concentration of catalase typically
153 correlates with the concentration of hydrogen peroxide. Our choice of catalase concentration
154 for liposomal application draws inspiration from a study conducted by Song et al. [13],
155 wherein they utilized the highest concentration of catalase at 40 mg/L.

156 The blank liposomes were prepared using the same procedure but without adding CAT or
157 H_2O_2 to the buffer. The resulting nanoparticles (NPs) were sterilized by filtration using a 0.22
158 μm sterile filter and then stored at 4°C.
159

160 2.4 Enzymatically crosslinked alginate hydrogel preparation

161 Alg-Ty hydrogels were prepared by the two-vial method at 37°C [21]. Briefly, one vial
162 containing 90μL of the gel precursors (Alg-Ty solution in PBS; 1, 2, or 3 %) and 10μL of HRP,
163 while the other containing 90μL of the gel precursors and 10μL of H_2O_2 were mixed and
164 gently stirred to homogenize and form the gel. The gelation time was recorded by the tube
165 inversion method [22]. The final concentration of HRP and H_2O_2 was 1 U/mL, and 1 mM,
166 respectively. To prepare liposomal Alg-Ty hydrogels, the desired concentration of CAT@Lip
167 or H_2O_2@Lip was added to the PBS solution.

168

169 2.5 CAT@Lip and H_2O_2@Lip characterization

170 The size, polydispersity index, and zeta potential of CAT@Lip and H_2O_2@Lip were measured
171 using the dynamic light scattering technique using the Zetasizer Nano ZS (Malvern
172 Instruments Limited, Worcestershire, UK). Eq. 1 was used to compute the CAT or H_2O_2
173 entrapment efficiency (EE %) [23].

174 $$\text{EE } (\%) = \left(\frac{W_{T-}\, W_F}{W_T}\right) \times 100, \qquad \text{(Eq. 1)}$$

175 Where WT is the initial amount of CAT or H_2O_2 used in total in the liposomes' preparation,
176 and WF is the amount of the unloaded reagents, which was detected in the supernatant after
177 centrifugation. The CAT concentration was determined using the ultraviolet (UV)
178 spectrophotometer technique (NanoDrop 2000/2000c, Thermo Fisher Scientific). The
179 quantitative evaluation of H_2O_2 generation is frequently carried out using the fluorometric
180 Amplex UltraRed /HRP assay [24, 25]. Briefly, a mixture of Amplex™ UltraRed reagent (100
181 μM) and HRP (1U/ml) was added to the H_2O_2 solutions. After 15 min incubation, the

182 fluorescent reaction products were quantified using a fluorometer (Multilabel reader, Victor
183 X4, Singapore).
184
185 2.6 Oxygen generation evaluation
186 We conducted an examination of the oxygen release profiles of the synthesized CAT@Lip,
187 H_2O_2@Lip, and H_2O_2@Lip in conjunction with CAT@Lip, all performed under hypoxic
188 conditions at pH 7 and room temperature. For this evaluation, we employed cell culture
189 media as the release medium, with the induction of hypoxia achieved by infusing pure
190 nitrogen into the media for a duration of 30 min. The oxygen release dynamics of H_2O_2@Lip
191 at a concentration of 1.65 mM, both in the presence and absence of 1.25 mg/mL of CAT@Lip,
192 were meticulously tracked utilizing a commercially available contactless oxygen sensor
193 (PreSens, Regensburg, Germany), as previously reported [26, 27]. Figure 4a illustrates the
194 procedure for measuring oxygen using the contactless oxygen sensor.

195 To study the potential of the H_2O_2 and CAT nanoparticles to generate oxygen, the CAT@Lip
196 and H_2O_2@Lip nanoparticles were added to a well of sealed 24 well-plate containing the
197 media and incubated in a hypoxia incubator chamber. To prevent degradation of H_2O_2 by
198 light and temperature, the release container (sealed 24 well-plate) was covered by aluminum
199 foil. The oxygen release of the synthesized nanoparticles was conducted in triplicate.
200
201 **2.7 Stability study**
202 To evaluate the stability of H_2O_2@Lip based on EE%, freshly synthesized samples were
203 washed three times with DPBS and incubated at 37˚C. Then, the EE% of the H_2O_2 was

204 evaluated after 1, 2, 4, and 24 h. Afterward, the stability of the H_2O_2@Lip was computed using
205 the following equation.

206 $$\text{Stability } (\%) = \left(\frac{EE_N}{EE_0}\right) \times 100, \qquad \text{(Eq. 2)}$$

207 Where the EE_0 is the EE% of the samples immediately evaluated after preparation and EE_N is
208 the EE% of the samples after incubation for "N" hours.

209

210 2.8 Hydrogel characterizations

211 2.8.1 Rheological properties

212 The rheological properties were investigated with a rheometer (Modular Compact
213 Rheometer MCR 302, Anton Paar, Graz, Austria) coupled with a parallel plate (25mm) using
214 oscillatory mode. The storage moduli (G') and the loss moduli (G") were recorded as a
215 function of the time, the strain, and the frequency using oscillatory tests [28]. An amplitude
216 sweep ranging from 0.01 to 1000 % was performed at a constant frequency of 1 Hz to
217 determine the linear viscoelastic region (LVR). The gelation kinetic was determined iso-
218 thermic gel time test frequency of 1 Hz and a strain of 0.01 % LVR at 37°C. The frequency
219 sweep test was carried out over the frequency range of 0.1 to 10 Hz at a constant strain of
220 1%. Moreover, the frequency and amplitude sweep tests were conducted on the liposomal
221 hydrogels (2 % Alg-Ty) to investigate the effect of liposome NPs on the hydrogel viscoelastic
222 properties.

223

2.8.2 Swelling ratio

The swelling ratio of hydrogels was investigated using the method previously described [15]. Briefly, the hydrogels (200 μL) were immersed in 10 mM PBS solution (pH=7.4) and incubated at 37 °C. At a predetermined time point, hydrogels were removed, and the excess water was removed by filter paper. The equilibrium swelling ratio was calculated by the following equation:

$$\text{Swelling ratio } (\%) = \left(\frac{W_1 - W_0}{W_0}\right) \times 100, \qquad \text{(Eq. 2)}$$

Where W_0 and W_1 are the weight of hydrogels before and after swelling, respectively.

2.8.3 Degradation assay

Following previous reports, the remaining mass behavior of the hydrogels with different Alg-Ty concentrations was investigated by measuring the weight of the hydrogels before and after immersing in PBS with a pH of 7.4 at 37.5°C [29]. Before starting the degradation assay, to swell completely, the hydrogels were soaked in PBS with a pH of 7.4 at 37.5°C for two days and weighed (Mi). Then, after predetermined time points, the hydrogels were withdrawn from the buffer and weighed after removing the surface water with a filtering paper (Md). The remaining mass of the hydrogels was calculated by the following equation.

$$\text{Remaining mass } (\%) = \frac{Mi}{Md} \times 100, \qquad \text{(Eq. 3)}$$

243 2.9 Human stromal cell isolation and culture

244 For this study, the ovaries from deceased multi-organ donors were collected following
245 approval from the Université Catholique de Louvain's Institutional Review Board for the use
246 of the human ovaries on May 25, 2019 (IRB reference 2018/19DEC/475). After procurement,
247 ovaries were immediately frozen [30]. For ovarian cell isolation, the ovarian samples were
248 thawed and digested using our routine protocols [31-33]. Briefly, the tissue fragments were
249 mechanically minced and then digested in DPBS, 0.28 Wünsch units/mL Liberase DH, and 8
250 Kunitz units/mL DNase. The mixture was pipetted every 15 minutes while being incubated
251 at 37°C for 75 minutes with 150 rpm of agitation. A solution of DPBS without Ca^{2+} and Mg^{2+}
252 containing 10% HI FBS was added in equal amounts to PBS without Ca^{2+} and Mg^{2+} to
253 inactivate the enzymes. The suspension was then successively filtered through 80 µm and 30
254 µm nylon net filters to remove the remaining particles. The finished suspension underwent
255 a ten-minute 500g centrifugation. Following cell counting with trypan blue and Bürker
256 chamber, the pellet was resuspended in a cell culture medium, including DMEM/F12, 10% HI
257 FBS, and 1% AA. The cells were then cultured at 37°C in a humid incubator with 5% CO_2. Cells
258 were subcultured once they reached confluence, with the culture media being changed every
259 other day.

260

261 2.10 Intracellular ROS generation

262 DCFH-DA probe and Nanolive super-resolution 3D microscopy was employed to measure
263 intracellular ROS levels after no treatment (control) or various treatments, including free
264 H_2O_2, CAT@Lip, H_2O_2@Lip, or CAT@Lip+H_2O_2@Lip. In the presence of ROS, DCFH-DA can

265 penetrate the cell and oxidize to form 2′,7′-dichlorofluorescein (DCF), which can be detected
266 using a green fluorescence detector [34].

267 H_2O_2, an oxidative agent, can induce cytotoxicity in mammalian cells due to diffusing into the
268 cells and causing DNA damage, depression of intracellular ATP, alterations to the
269 cytoskeleton and plasma, activation of the glutathione redox cycle, the hexose
270 monophosphate shunt, and rapid increases in intracellular calcium [35-38]. Briefly, a 20 M
271 working solution was produced by diluting a 5 mM DCFH-DA stock solution (in DMSO) in
272 a DMEM medium. CAT@Lip, H_2O_2@Lip, or CAT@Lip plus H_2O_2@Lip were added after 30
273 minutes of incubation with the DCFH-DA working solution. Fluorescence was subsequently
274 observed using super-resolution 3D microscopy after three PBS solution washes (CX-A
275 Imaging Platform; Nanolive, Tolochenaz, Switzerland).

276

277 2.11 *In vitro* cell experiment

278 2.11.1 Biocompatibility

279 To evaluate the effect of liposomal encapsulation on H_2O_2 cytotoxicity and biocompatibility
280 of CAT@Lip, isolated stromal cells (2×10^4 cells/well) were treated in triplicate with either
281 H_2O_2@Lip for 24 h, or initially incubated with CAT@Lip for 4 h before being supplemented
282 with various doses of H_2O_2@Lip for an additional 20 h of incubation. Untreated cells and wells
283 containing just medium were used as the positive and negative controls, respectively, before
284 the cell viability assay.

285

286 2.11.2 Evaluation of oxygen-releasing liposomal hydrogel

287 A total of 30,000 stromal cells were encapsulated in 40 μl of Alg-Ty hydrogel with or without
288 H_2O_2@Lip/CAT@Lip. Then, the hydrogels were exposed to hypoxia for another 72 h. A group
289 of stromal cell-embedded Alg-Ty hydrogel in normoxia was used as the positive control, and
290 cell-free Alg-Ty hydrogel with or without H_2O_2@Lip/CAT@Lip was used as the negative
291 control. This experiment was performed in triplicate.

292

293 2.11.3 Cell viability assay

294 Cell viability was determined using the PrestoBlue™ HS cell viability reagent metabolic test
295 for biocompatibility and *in vitro* studies. Resorufin, a red fluorescent substance that can be
296 quantitatively evaluated to ascertain cell viability, is produced when PrestoBlue, a resazurin-
297 based solution, is decreased inside the mitochondria of live cells [34]. Free stromal cells and
298 hydrogels containing or not stromal cells were incubated for 1 and 3 h, respectively, in a cell
299 medium containing 10% PrestoBlue™ reagent. Thereafter, the media was removed and
300 analyzed by a spectrometer (Multilabel reader, Victor X4, Singapore) with an excitation
301 wavelength of 560 nm and an emission wavelength of 620 nm. The positive and negative
302 controls for each study were used for normalization to have 100% and 0% viability,
303 respectively.

304 The viability of cells treated with the highest concentration was assessed using the
305 LIVE/DEAD™ assay [39]. Briefly, cells were treated with 2 mmol/l calcein-AM and 5 mmol/l
306 ethidium homodimer-I in d-PBS for 45 minutes at 37°C in the dark. Live and dead cells were

307 visualized using an inverted fluorescence microscope with a green fluorescence filter (ex/em
308 495/515 nm) for live cells and a red fluorescence filter (ex/em 495/635 nm) for dead cells.

309

310 2.11.4 Immunofluorescence analysis

311 Alg-Ty hydrogels with or without H_2O_2@Lip/CAT@Lip were fixed in a 4% formaldehyde
312 solution before embedding in paraffin. Five-micrometer-thick sections were cut and placed
313 on Superfrost Plus slides (Menzel-Glaser, Germany). To evaluate the effect of hypoxia on the
314 apoptosis of the encapsulated stromal cells in the hydrogels, caspase-3 immunofluorescence
315 analysis was employed [38]. The tissue sections were deparaffinized using Histosafe
316 (Yvsolab SA, Belgium) and rehydrated in isopropanol. Antigen retrieval was performed by
317 heating the sections in citrate buffer and Triton X-100 in a microwave for 20 minutes. To
318 block non-specific binding sites, the sections were incubated with a solution of TBS/Tween
319 containing 10% NGS and 1% BSA for 30 min. The sections were then incubated overnight at
320 4°C with a polyclonal anti-caspase-3 primary antibody (1:200). After washing the slides with
321 TBS/Tween 0.1%, the sections were incubated for 40 min with Alexa FluorTM 488 goat anti-
322 rabbit IgG. Finally, the sections were mounted with fluorescent mounting medium on glass
323 slides and analyzed using a confocal microscope (LSM800; Zeiss) equipped with laser lines
324 at 455, 488, and 594 nm.

325

326 2.12 Statistical analysis

327 One-way ANOVA followed by Tukey's multiple comparison posthoc test was employed to
328 statistically examine the quantitative data using GraphPad Prism version 9.1.2. Each data

329 point is represented as mean ± standard deviation (SD). Statistics were considered significant
330 for *p*-values under 0.05 and the error bars in graphs represent the standard deviation of one
331 sample.

332

333

334 **3 Results and discussion**

335 3.1 CAT@Lip and H_2O_2@Lip characterizations

336 The size, Zeta potential**,** and polydispersity index of CAT@Lip and H_2O_2@Lip were
337 determined using the DLS instrument (Table 1). DLS detects the diffusion of the particles'
338 Brownian motion and uses the Stokes-Einstein relationship to calculate the size and
339 polydispersity index [40]. The polydispersity index values of CAT@Lip and H_2O_2@Lip, which
340 indicate the quality of the nanoparticles following the size distribution, were lower than 0.2
341 and between 0.2-0.4, respectively, classifying them as monodisperse and nearly
342 monodisperse liposomes [41]. In the field of biomedical science, a polydispersity index of 0.3
343 or less is considered acceptable for lipid-based carriers such as liposomes and indicates a
344 homogenous population [42]. CAT@Lip and H_2O_2@Lip had Zeta potentials of -6.00±0.10 and
345 -14.95±0.05, respectively, indicating that they were negatively charged and relatively stable
346 [43]. Furthermore, the encapsulation efficiency of CAT and H_2O_2 were 80.235±1.572 % and
347 70.421±4.691 %, respectively. It has been reported that the activity of free CAT had
348 decreased by 90% after 24 days, whereas CAT@Lip did not exhibit any deactivation of
349 catalase within the same time frame [44].

350 Attaining a high EE for hydrophilic agents within liposomes presents a daunting challenge,
351 although not an insurmountable one. EE of hydrophilic drugs in liposomes is influenced by
352 several parameters that warrant optimization. Based on the literature and our experience
353 with nanovesicular drug delivery systems, we tried to minimize all the limiting parameters.
354 Some of these criteria are: (i) augmenting the phospholipid concentration during film
355 preparation is a common strategy to enhance EE. Notably, BSA-loaded liposomes, created
356 using 150 mM DPPC, exhibited an impressive EE of 78% [45]; (ii) maintaining a cholesterol-
357 to-phospholipid ratio of 1:2 aids in achieving a delicate balance between stability and EE. Guo
358 et al. [46], through RSM-based optimization of liposomes, highlighted that a 1:2 ratio yielded
359 the optimal EE of 77.29%; (iii) while PEG-modified phospholipids are frequently employed
360 to prolong blood circulation in many studies, their use is not necessary for tissue engineering
361 applications. It is worth noting that although PEG augmentation enhances the EE of lipophilic
362 drugs, its incorporation significantly constrains the entrapment of hydrophilic drugs [47].

363 Table 1. Size, polydispersity index, zeta potential, and entrapment efficiency of CAT@Lip and
364 H_2O_2@Lip.

	Size (nm)	Polydispersity index	Zeta potential (mV)	Encapsulation efficiency (%)
CAT@Lip	142.54±3.23	0.19±0.01	-6.00±0.10	80.23±1.57
H_2O_2@Lip	159.77±4.03	0.33±0.01	-14.95±0.05	70.42±4.69

365 Catalase-loaded liposomes (CAT@Lip) and H_2O_2-loaded liposomes (H_2O_2@Lip).

366

367 3.2 Hydrogel formation

368 In our study, we decided to use alginate as 3D matrix. Alginate boasts a linear copolymer
369 structure consisting of two distinct monomers: guluronic acid (G) and mannuronic acid (M).
370 This composition confers versatile functionality and exceptional biocompatibility upon
371 alginate. These inherent qualities enable effective interactions with both cells and tissues,
372 establishing alginate as a highly promising biomaterial with extensive applicability in diverse
373 biomedical domains. Furthermore, in addition to its biocompatibility, the simplistic
374 modification of alginate through incorporation of phenol-functionalized groups is
375 noteworthy. This particular characteristic enables us to employ enzyme-mediated
376 crosslinking utilizing horseradish peroxidase and hydrogen peroxide, a capability that
377 enriches the versatility of our experimental approach.

378 Before hydrogel formation, alginate was functionalized with tyramine groups using amide
379 coupling chemistry (Fig. **1**a). The success of alginate conjugation was confirmed by 1H NMR
380 and UV-vis analyses. The 1H NMR spectrum exhibited two new peaks at 6.6-7.2 ppm,
381 corresponding to the aromatic ring protons of the phenol groups, indicating successful
382 tyramine conjugation into the alginate backbone (Fig. **1**b) [48]. Moreover, the UV spectra
383 exhibited a new peak at 275 nm for Alg-Ty compared to the Alg spectrum (Fig. **1**c), confirming
384 the presence of phenol groups and successful conjugation of tyramine into the alginate
385 backbone [49]. To synthesize oxygen-releasing Alg-Ty hydrogels, CAT@Lip and/or
386 H_2O_2@Lip were added to the Alg-Ty solution. The chemical structures of the lipids
387 comprising the liposome bilayer, including phospholipids and cholesterol, are shown in
388 Figure 1d.

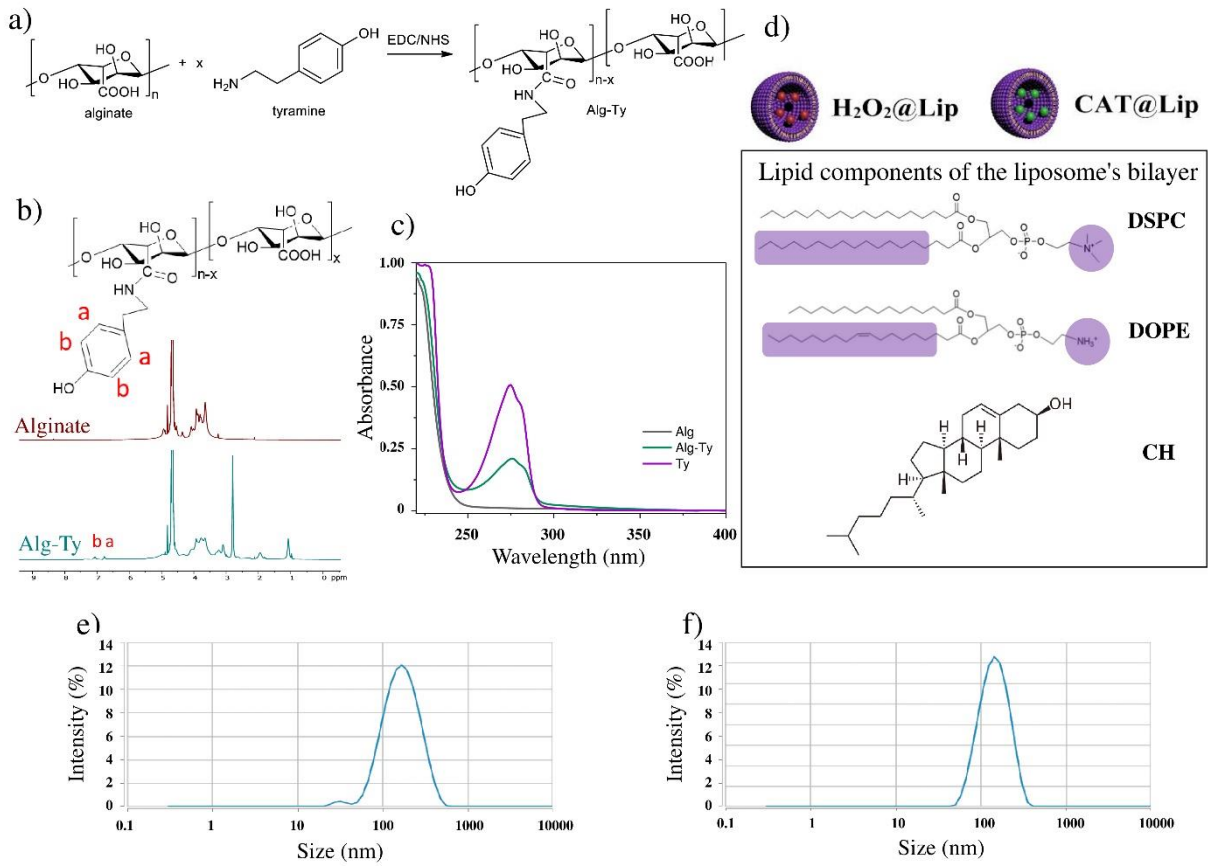

Figure 1. **Alginate-tyramine hydrogel components structure, NMR, Uv-vis spectra, CAT@Lip/H_2O_2@Lip structure, and DLS analysis.** Synthetic scheme for alginate-tyramine (Alg-Ty) conjugates using EDC/NHS coupling chemistry (a); ^{1}H NMR spectra of alginate (Alg), Alg-Ty (b); Uv-vis spectra of Alg, Alg-Ty, and tyramine (Ty) (c); the lipid components of liposomes bilayer, including (i) the phospholipids; 1,2-distearoyl-sn-glycero-3-phosphocholine (DSPC) and 1,2-dioleoyl-sn-glycero-3-phosphoethanolamine (DOPE) (their differences are highlighted), and (ii) the cholesterol (CH) (d): and the size distribution of CAT@Lip (e) and H_2O_2@Lip (f) from DLS analysis.

Enzymatically crosslinked alginate-based hydrogels were produced by using aqueous solutions of alginate-tyramine (Alg-Ty) in the presence of HRP and H_2O_2. H_2O_2 acts as an oxidizing substrate for HRP, which converts the ferric heme of the enzyme to the ferryl state. The activated HRP reacts with the phenol groups conjugated to the alginate backbone, resulting in the production of phenoxy radicals. These phenoxy radicals then react and form stable covalent C-C or C-O bonds through a radical coupling reaction, leading to rapid hydrogel formation (Fig. 2a,b) [50]. Investigating the effect of the polymer concentration on the gelatin time revealed that increasing the Alg-Ty from 1 to 3 wt% reduced the gelation time from 114.3 ± 5.6 to 34.3 ± 3.2 s indicating the controllable gelation time of the Alg-Ty hydrogel (Fig. 2c). This phenomenon can be explained by the increase in the amount of phenolic content due to the increased Alg-Ty concentration, which leads to an increase in phenoxy radicals and, consequently, an acceleration in the gelation time of the hydrogel [51].

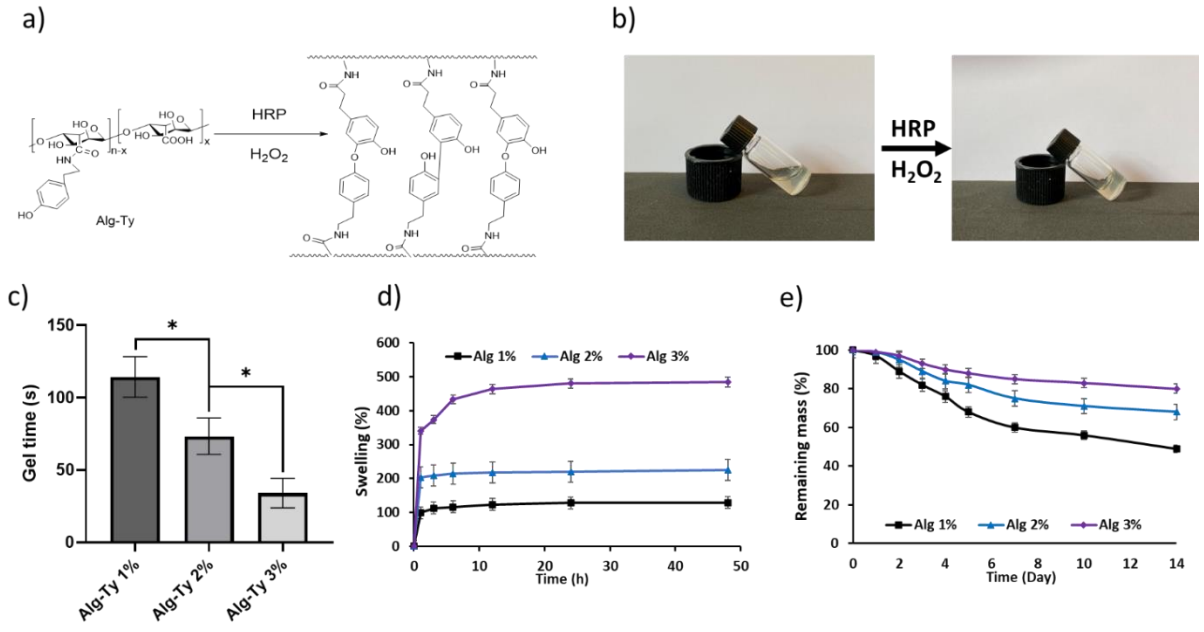

412 **Figure 2. Alg-Ty hydrogel characterization, including gelation time, swelling ratio, and**
413 **degradation.** Synthetic scheme for hydrogel preparation using Alg-Ty in the presence of
414 horseradish peroxidase (HRP) and hydrogen peroxide (H_2O_2) (a); Photograph of the
415 enzymatically crosslinked Alg hydrogel (b); gelation time of the Alg-Ty hydrogel with
416 different polymer concentrations (1, 2, 3 wt%) at a constant concentration of HRP (1 U/mL)
417 and H_2O_2 (1 mM) (c); the welling ratio of Alg-Ty hydrogels with different polymer
418 concentration (1, 2, 3 wt%) (d); Degradation behavior of Alg-Ty hydrogels with different
419 polymer concentration (1, 2, 3 wt%) (e).

420

421 3.3 Hydrogel characterization

422 The physicochemical properties of Alg-Ty hydrogels were investigated to characterize the
423 effect of Alg-Ty concentration (1, 2, and 3 wt%). Swelling and degradation behavior were
424 examined and the results are shown in Figure 2d,e. Increasing the Alg-Ty concentration from
425 1 to 3 wt% resulted in an augmentation in the ultimate swelling of the hydrogels from
426 128.75% to 485.18%. Additionally, the swelling rate of the hydrogels enhanced as the Alg-Ty
427 concentration increased. After one hour of swelling, Alg-Ty 3% showed a swelling rate **of**
428 138.70% and 241.98% higher than Alg-Ty 2% and Alg-Ty 1%, respectively. This could be due
429 to the higher density of polar groups of Alg-Ty in the same volume of the hydrogels. The
430 increase in the swelling of the hydrogels by augmenting the Alg-Ty concentration is similar
431 to the enhancement reported for Alg-based hydrogels by increasing the Alg concentration
432 [52].

433 In addition, the stability of the hydrogel in the degradation buffer (PBS, pH 7.4, and
434 temperature of 37.5°C) was improved by increasing the Alg-Ty concentration from 1 to 3
435 wt%. After 14 days of incubation in the degradation buffer, the remaining mass of Alg-Ty 1%,
436 Alg-Ty 2%, and Alg-Ty 3% was 49.92%, 68.19%, and 80.13%, respectively. The increase in
437 Alg-Ty concentration provides more phenol sites for enzymatic crosslinking, resulting in a
438 higher total amount of Alg-Ty in the same volume and thus increasing the stability of the
439 hydrogels.

440

441 3.4 Rheological properties

442 The effect of Alg-Ty concentration and nanoparticles on the hydrogels' viscoelastic
443 properties was investigated by rheological measurement (Fig. 3). First, the gelation kinetics
444 of the Alg-Ty hydrogel (1, 2, and 3 wt%) was examined at a constant concentration of HRP (1
445 U/mL) and H_2O_2 (1 mM) (Fig. 3a). The gelation immediately started after the enzyme
446 activation by H_2O_2 [53]. The storage modulus of hydrogels spontaneously augmented, and
447 the results showed that increasing the Alg-Ty concentration from 1 to 3 % enhanced the
448 storage modulus from 657 to 4627 Pa after 10 minutes due to more phenolic content, leading
449 to the formation of more phenol-phenol (C-C, or C-O) bonds, resulting in higher crosslinking
450 density. The frequency results at a constant strain (1 %) (Fig. 3b) demonstrated a storage
451 modulus independent of frequency, indicating a typical stiff gel behavior due to the presence
452 of covalent interactions [54]. Besides, similar to the gelation kinetic, the effect of the polymer
453 concentration was observed on the storage and loss moduli of the hydrogels. Moreover, the
454 amplitude sweep test (Fig. 3c) indicated the LVR for the hydrogels up to 20% strain.
455 Importantly, 1% and 2% Alg-Ty exhibited a critical strain at 149 %, while increasing the

456 concentration to 3% decreased the critical strain to 109%, which could be due to the
457 enhancement of the crosslinking density, which resulted in brittleness of the hydrogel [55].
458 According to the viscoelastic and gelation time result, the 2% Alg-Ty hydrogel was chosen for
459 further investigation. Indeed, long and short gelling times of 1% (114.3 ± 5.6 s) and 3% Alg-
460 Ty (34.3 ± 3.2 s), respectively, can hinder the encapsulation of stromal cells. Moreover, the
461 low G' of 1% Alg and the high stiffness and low flexibility of 3% Alg may adversely affect the
462 proliferation and viability of the stromal cell. Hence, CAT@Lip, and H_2O_2@Lip were
463 incorporated into the 2% Alg-Ty. Then, the effect of NPs' incorporation into the 2% Alg-Ty
464 was investigated by oscillatory tests (Figs. 3d,e). The CAT@Lip, H_2O_2@Lip, and their mixture
465 were incorporated into the hydrogel precursor (2% Alg-Ty) before the hydrogel formation
466 with a final concentration of 40 mg/L for CAT@Lip, and 50 mM for H_2O_2@Lip. The frequency
467 sweep test revealed no significant difference in the storage (G') and loss moduli (G'') of
468 hydrogels after the NPs' incorporation (Fig. 3d). All of the hydrogels exhibited a frequency-
469 independent G' and G'', indicating that the NPs' incorporation did not affect the hydrogel
470 formation. Moreover, the result showed that integrating the CAT@Lip, and H_2O_2@Lip led to
471 improvement in the hydrogel G'. Indeed, the G' of the 2% Alg-Ty (1022 Pa) increased to 1064,
472 1304, and 1376 Pa after adding H_2O_2@Lip, CAT@Lip, and the mixture of
473 H_2O_2@Lip/CAT@Lip, respectively (Fig 3d). The result indicated that the liposome NPs could
474 act as a reinforcing agent to improve the hydrogel mechanical properties, probably by the
475 hydrogen bonding formation with an alginate backbone [56]. Elkhoury et al. [57] reported
476 that incorporating nanoliposomes could significantly increase the GelMA hydrogel due to the
477 formation of additional hydrogen bonding with the hydrogel network. Moreover, the
478 amplitude sweep test (Fig. 3e) demonstrated no significant difference in moduli, LVR, and the

critical strain of the hydrogels after the NPs incorporation compared to the native Alg-Ty hydrogel. Hence, these results suggest that the NPs incorporation did not interfere with the HRP-mediated cross-linking.

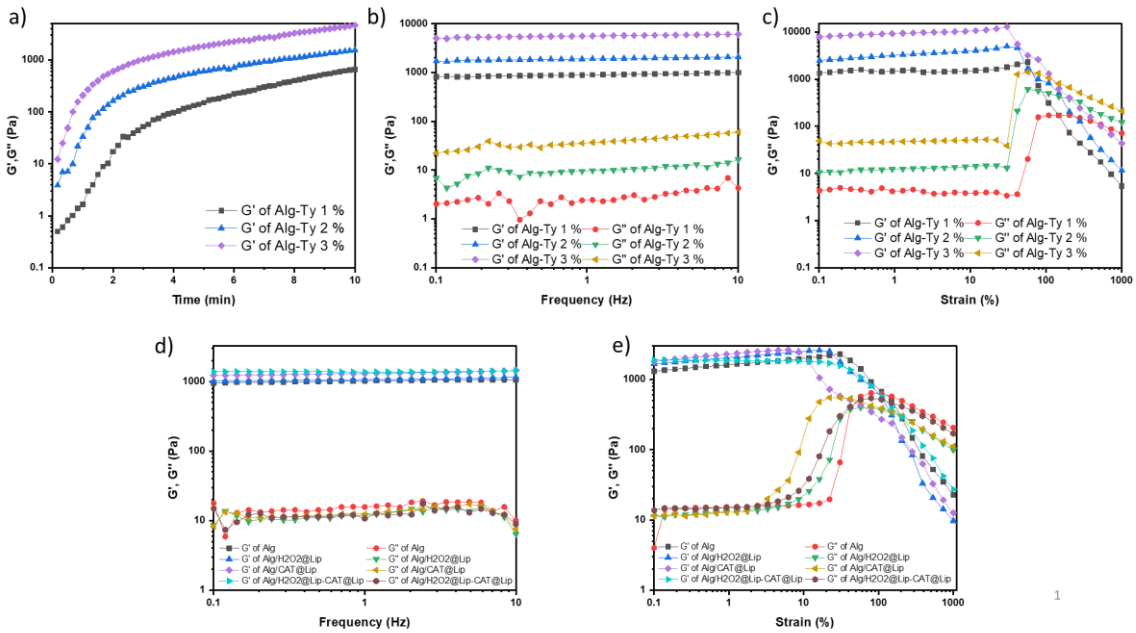

Figure 3. The effect of Alg-Ty concentration and nanoparticles on the hydrogels' viscoelastic properties. Viscoelastic properties of alginate-tyramine hydrogels. Gelation kinetic of Alg-Ty hydrogels with different concentrations (1, 2, and 3 wt%) (a); Frequency sweep test of Alg-Ty hydrogels with different concentrations (1, 2, and 3 wt%) at a constant strain of 1% (b); Amplitude sweep test of Alg-Ty hydrogels with different concentration (1, 2, and 3 wt%) at a constant frequency of 1 Hz (c); Frequency sweep test of Alg-Ty hydrogels containing CAT@Lip, H_2O_2@Lip, and CAT@Lip, H_2O_2@Lip mixture at a constant strain of 1% (d); Amplitude sweep test of Alg-Ty hydrogels containing CAT@Lip, H_2O_2@Lip, and CAT@Lip, H_2O_2@Lip mixture at a constant frequency of 1 Hz (e).

493 **3.5 Oxygen generation and H_2O_2@Lip stability**

494 The oxygen-producing strategy in biomaterials can either directly convert hydrogen
495 peroxide (H_2O_2) into molecular oxygen or dissolve solid peroxides in an aqueous solution to
496 release H_2O_2 and produce molecular oxygen [58]. While the utilization of solid peroxides has
497 been extensively investigated, there is a concern regarding the release of cations into the
498 solution, potentially exerting deleterious effects on certain cell types [59]. We hypothesized
499 that H_2O_2 and CAT diffuse out from liposomal systems, and H_2O_2, in the presence of CAT,
500 decomposes into water and molecular oxygen. Figure 4b displays a schematic representation
501 of the oxygen generation strategy. We investigated the release of oxygen generated via the
502 decomposition of the incorporated H_2O_2 in the nanoparticles with and without CAT@Lip and
503 compared it with the oxygen release of H_2O_2 alone to study the controllability of Lip
504 nanoparticles on oxygen generation. When a single dose of H_2O_2 was added to the release
505 media, 4.32 μM of oxygen was produced within the first hour. In contrast, the concentration
506 of oxygen generated by H_2O_2@Lip was 0.69 μM at the same time. The maximum
507 concentration of oxygen for H_2O_2@Lip was observed at minute 235, which was 1.86 μM.
508 Therefore, Lip nanoparticles can control the oxygen release by controlling the release of
509 H_2O_2. The loaded CAT in the Lip nanoparticles (CAT@Lip) accelerated and increased the
510 oxygen release of H_2O_2@Lip by enhancing the decomposition rate of H_2O_2 (54). The
511 maximum oxygen concentration reached 12.70 μM at minute 145 from 1.86 μM at minute
512 235 for H_2O_2@Lip with CAT@Lip. However, CAT@Lip was not able to produce oxygen in the
513 absence of H_2O_2 (Fig. 4c). Moreover, since free H_2O_2 can quickly decompose by CAT@Lip,
514 which may potentially lead to O_2 excess supply exposure and cause a hyperoxia condition
515 [13], H_2O_2@Lip stability is one of the key issues with the liposomal oxygenation strategy.

516 Therefore, we investigated the stability of H_2O_2@Lip based on the EE% of H_2O_2 and the
517 results demonstrated that while 15.51 ± 1.42 % of loaded H_2O_2 is released in the first four
518 hours of incubation, 65.94 ± 2.16% of H_2O_2 is still encapsulated in the liposomes after 24h
519 (Fig. 4d).

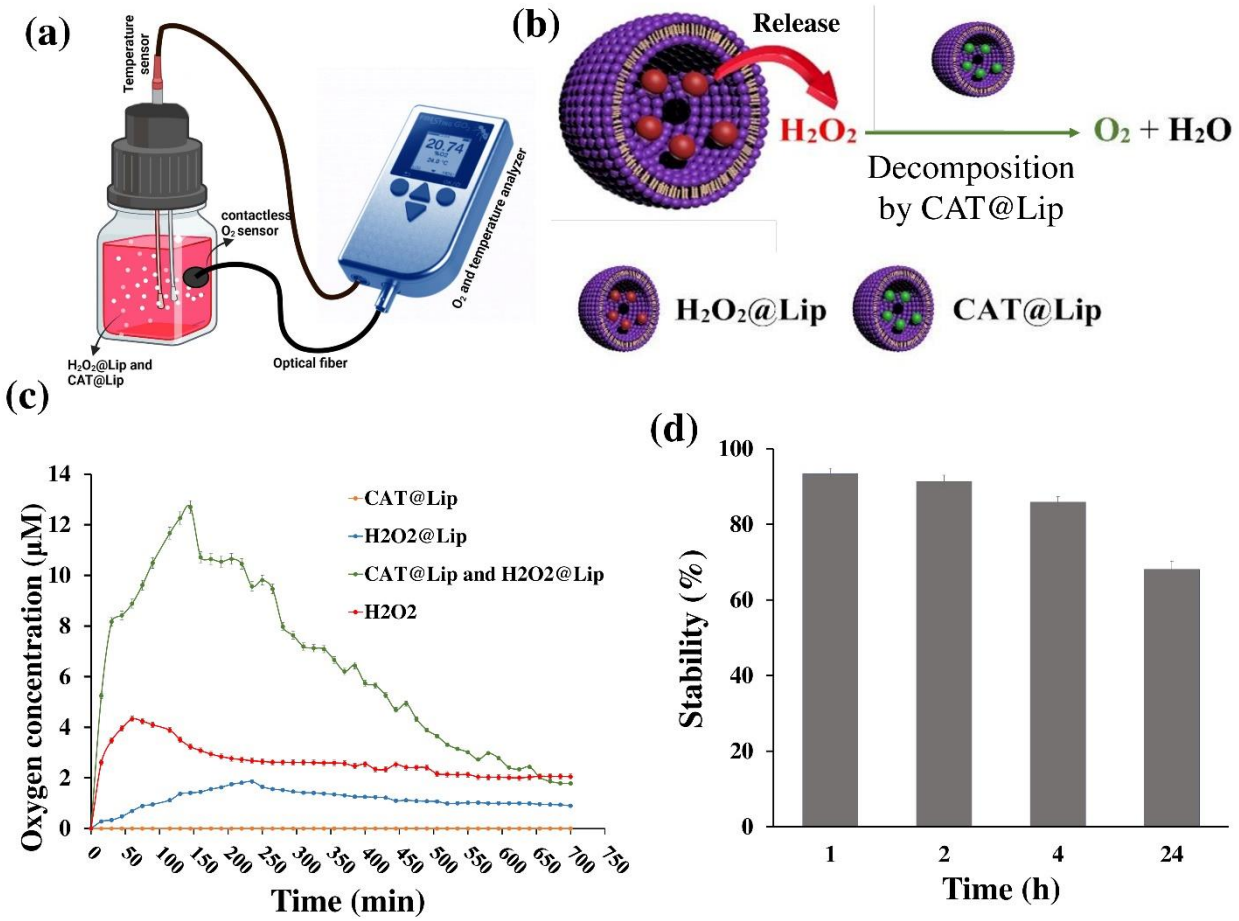

520

521 **Figure 4. CAT@Lip and H_2O_2@Lip oxygen release profile.** The schematic represents the
522 procedure of monitoring oxygen by the contactless oxygen analyzer (a) (Figure created with
523 biorender.com). The schematical illustration of H_2O_2 release from H_2O_2@Lip and O_2
524 generation after the decomposition of released H_2O_2 by CAT@Lip (b), the oxygen release
525 profile from CAT@Lip, H_2O_2@Lip, free H_2O_2, and CAT@Lip/H_2O_2@Lip (c), and the stability of
526 H_2O_2@Lip during 24h incubation in DPBS (d).

527

528 3.6 Intracellular ROS generation

529 In this study, we aimed to quantify ROS production by measuring the FITC fluorescence
530 probe, which has peak excitation and emission wavelengths of 495 nm and 519 nm. Our
531 results indicate that the ROS production after treatment with free H_2O_2 and H_2O_2@Lip were
532 significantly higher than the control (Figs. 5a-c). Both necrotic and apoptotic cell death can
533 result from intracellular ROS due to the oxidation of any biological molecule within a cell [60].
534 In contrast, there was no significant difference between the ROS generated in stromal cells
535 after treatment with CAT@Lip and the control, indicating that CAT@Lip itself does not cause
536 cytotoxic intracellular ROS. Furthermore, in the CAT@Lip+ H_2O_2@Lip group, the normalized
537 intensity of DCF was comparable to that of the control and CAT@Lip (Fig. **5**c), suggesting that
538 the cytotoxic H_2O_2 released from H_2O_2@Lip was significantly decomposed by CAT@Lip. The
539 decomposition reaction is quite rapid; in one minute, one mol of CAT, as an abundant natural
540 enzyme, can decompose 500 million mol of H2O2 into water and oxygen.

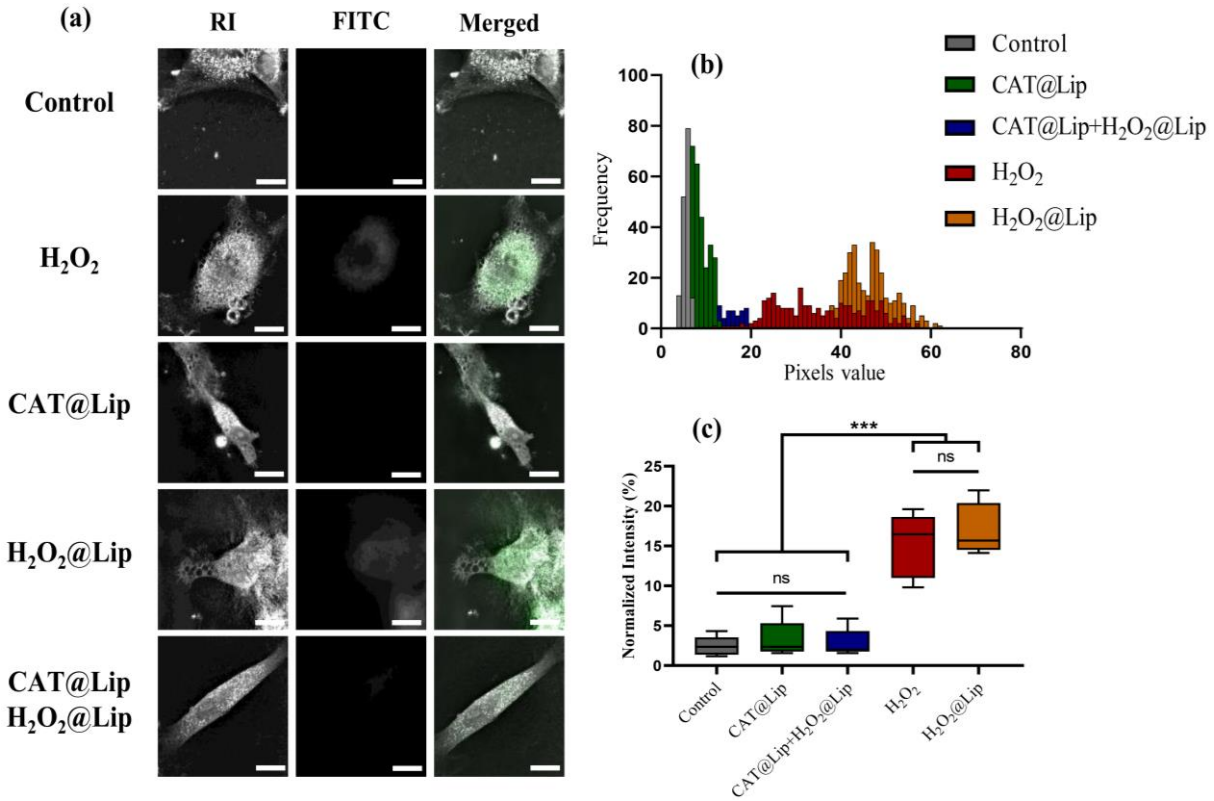

541

542 **Figure 5. Intracellular ROS generation of free H_2O_2, CAT@Lip, H_2O_2@Lip, and**
543 **CAT@Lip/H_2O_2@Lip mixture.** ROS generation in stromal cells before (control) or after
544 treatment by free H_2O_2, CAT@Lip, H_2O_2@Lip, and CAT@Lip/H_2O_2@Lip mixture (a); The
545 histograms of the frequency distribution of intracellular green pixels value (b); The
546 normalized value of the green intensity in the cells from the control, free H_2O_2, CAT@Lip,
547 H_2O_2@Lip, and CAT@Lip/H_2O_2@Lip mixture (c) (RI: refractive index, ns: not significant, ***
548 P<0.001).

549

550 3.7 *In vitro* cell experiment

551 In this study, we employed isolated ovarian stromal cells as a representative illustration of
552 human primary cells. In a previous study, we conducted fluorescence-activated cell sorting

553 on these isolated ovarian stromal cells, revealing that those supplemented with FBS exhibited
554 the expression profile CD31-, CD34-, CD73+, and CD90+. Consequently, these cells can be
555 classified into three distinct categories: fibroblasts, mesenchymal stem cells, and pericytes
556 [32]. The cytotoxicity of free H_2O_2 and H_2O_2@Lip on the stromal cells was evaluated after 20
557 h treatment by different H_2O_2 concentrations (0.39, 1.56, 6.25, 25, 50 mM). As expected, even
558 at the lowest concentrations (0.39 mM), free H_2O_2 had a noticeable influence on stromal cell
559 death (Fig. 6a1,a2). The cytotoxicity of H_2O_2@Lip started from 1.56 mM, showing that
560 liposomal encapsulation reduced the cytotoxicity of H_2O_2. However, the cell viability was still
561 significantly reduced at high concentrations of H_2O_2@Lip (Fig. 6b1,b2). Indeed, in the
562 absence of catalase, cytotoxic free hydroxyl radicals from H_2O_2 are detrimental to the cells
563 [6]. The biocompatibility assay on CAT@Lip showed no significant adverse effect on cell
564 viability, even at the highest dose (40 mg/L) after 24 hours of incubation (Fig. 6c1,c2).
565 Interestingly, when stromal cells were first incubated with nontoxic CAT@Lip for 4 hours
566 and then with H_2O_2@Lip for another 20 hours, there was no noticeable reduction in cell
567 viability even at high concentrations of H_2O_2@Lip (Fig. 6d1,d2). These results suggest that
568 the cytotoxicity of H_2O_2 can be effectively eliminated by decomposition with CAT@Lip.

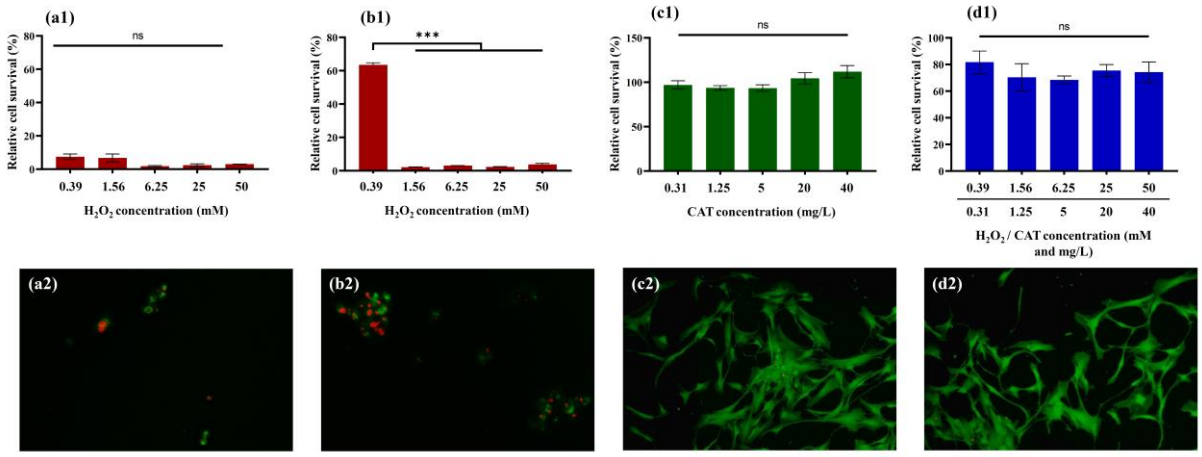

569

570 **Figure 6. *In vitro* cytotoxicity assessment using PrestoBlue and LIVE/DEAD cell**
571 **viability assays.** Cytotoxicity of free H_2O_2 (a1) and H_2O_2@Lip (b1); biocompatibility of
572 CAT@Lip (c1) and CAT@Lip/H_2O_2@Lip mixture (d1). LIVE/DEAD assay on stromal cells
573 treated by 50 mM free H_2O_2 (a2), 50 mM H_2O_2@Lip (b2), 40mg/L CAT@Lip (c2), and the
574 mixture of 40mg/L CAT@Lip and 50 mM H_2O_2@Lip (d2). (ns: not significant, *** $P<0.001$).

575

576 The rheological properties of Alg-Ty at different concentrations (1, 2, and 3 wt%) were
577 examined, and Alg-Ty at 2% with or without liposomal systems was selected based on the
578 most suitable stiffness, gelling time, and viscoelastic properties. The stromal cells were then
579 embedded in 2% Alg-Ty with or without liposomal systems (40 mg/L CAT@Lip and 50 mM
580 H_2O_2@Lip). To determine the effect of the oxygenation systems on the apoptosis status of
581 stromal cells, the expression of caspase-3 was examined on day 3 using immunofluorescence
582 analysis (Fig. 7a). The results showed a significant expression of caspase-3 in cell-embedded
583 hydrogels under hypoxia conditions, whereas the apoptosis rate of cells embedded in Alg-Ty
584 with oxygenation systems was similar to that of the control group under normoxia conditions
585 (Fig. 7b).

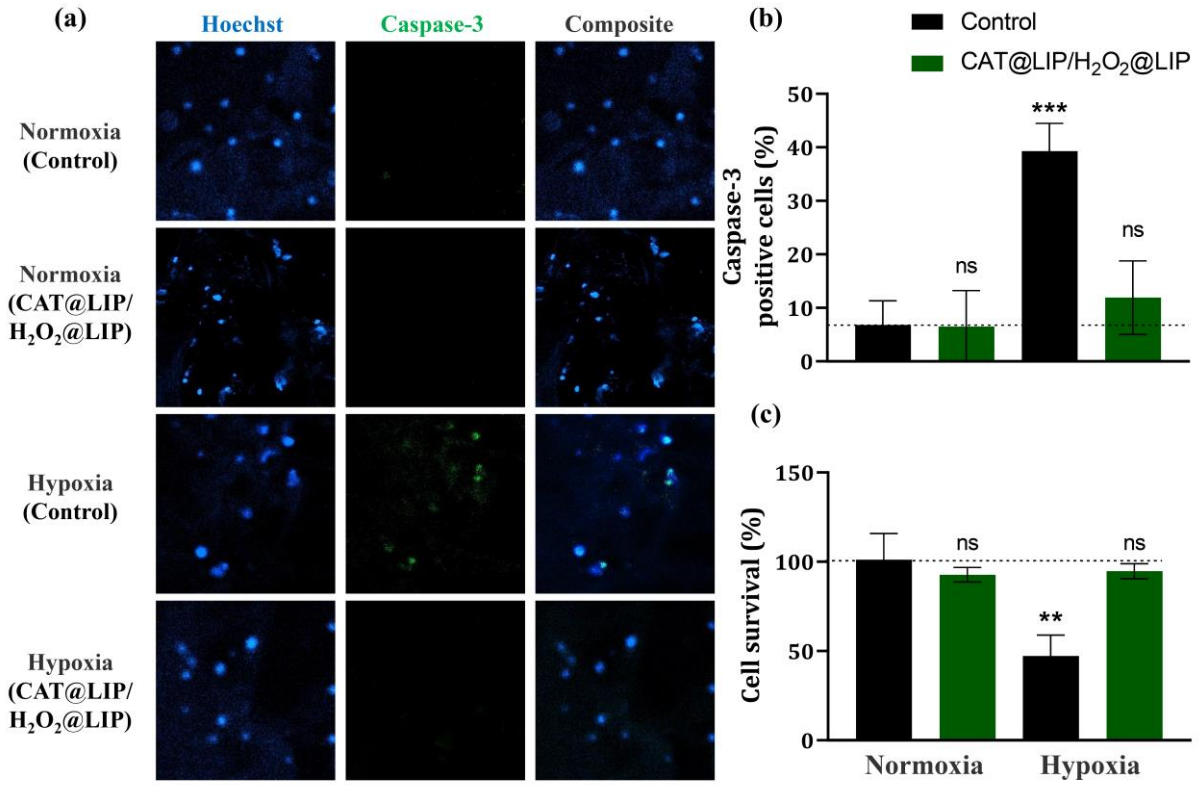

586

587 **Figure 7.** A**poptosis, and survival of stromal cells embedded in Alg-Ty hydrogel under**
588 **normoxia and hypoxia conditions.** Caspase-3 immunofluorescence analysis (a), the
589 apoptosis assay's quantification (b), and the viability assay (c) of stromal cells embedded in
590 Alg-Ty hydrogel without (control) or with the oxygenation system (CAT@Lip/H_2O_2@Lip)
591 after 72 h incubation in normoxia or hypoxia conditions (ns: not significant, ** $P<0.01$, ***
592 $P<0.001$).

593

594 According to the PrestoBlue™ analysis, the cell viability was significantly lower in the
595 hydrogels without oxygen-releasing systems that were incubated in a hypoxia incubator,
596 while the cell viability in the 2% Alg-Ty with liposomal systems was similar to that of
597 hydrogels incubated under normal conditions, even when incubated under hypoxic

conditions. This indicates that the released oxygen from the liposomal systems was able to counteract the negative effects of hypoxia on the embedded stromal cells (Fig. 7c). The decomposition of hydrogen peroxide to oxygen and water in the presence of catalase has been employed using various biomaterials to overcome hypoxic and ischemic conditions [6, 8, 61]. For example, Abdi et al. reported the use of poly(lactide-co-glycolide) (PLGA)-based H_2O_2 micro-systems encapsulated with alginate-catalase as oxygen-releasing biomaterials [6]. In their study, the catalase-infused alginate facilitated the conversion of hydrogen peroxide into oxygen and water without producing any damaging radicals that could have otherwise impacted cell viability. Similarly, other studies have shown that H_2O_2 released from PLGA microspheres and decomposed by catalase can release oxygen for at least two weeks, improving the survival and proliferation of cardio-sphere-derived cells [8].

4 Conclusion

This study demonstrates the potential of alginate-tyramine hydrogels with CAT@Lip and H2O2@Lip for in vitro cell culture under hypoxic conditions. The rheological properties of Alg-Ty hydrogels were enhanced with the incorporation of liposomal systems, and the cell viability was significantly lower in hydrogels without oxygen-releasing systems that were incubated in a hypoxia incubator. However, the cell viability in the 2% Alg-Ty with liposomal systems was similar to that of hydrogels incubated under normal conditions, even when incubated under hypoxic conditions. This indicates that the released oxygen from the liposomal systems was able to counteract the negative effects of hypoxia on the embedded

stromal cells. These results suggest that our liposomal oxygen-releasing systems embedded in biocompatible hydrogels could be a viable option for tissue engineering applications.

Authors' contributions

S.M. and A.D. wrote the study concept, designed and performed the experiments, created the figures, wrote the first draft of the article, and did the statistical analysis. H.J. and P.G.B. participated in the concept of the study, performing the experiments and writing the manuscript. A.S. reviewed and revised the manuscript. C.A.A. supervised the project, and reviewed and revised the manuscript. The final article and order of authorship have been approved by all authors.

Declaration of Competing Interest

The authors declare that they have no known competing financial interests or personal relationships that could have appeared to influence the work reported in this paper.

Acknowledgments

We deeply thank the Kidney and Pancreatic Transplantation Unit of UCLouvain's Saint-Luc Hospital for donating ovaries for this study. This study was supported by grants from the Foundation Louvain (Ph.D. scholarship awarded to S.M., as part of a legacy from Mr. Frans Heyes, and Ph.D. scholarship awarded to A.D. as part of a legacy from Mrs. Ilse Schirmer), Innoviris Brussels (Ph.D. scholarship awarded to H.J.), and Fonds National de la Recherche Scientific de Belgique (FNRS) grant number 38351, 2021 awarded to P.G.B.

Data availability

Data will be made available on request.

5 References

[1] A. Khademhosseini, R. Langer, A decade of progress in tissue engineering, Nature protocols, 11 (2016) 1775-1781.

[2] N. Ashammakhi, M.A. Darabi, N.S. Kehr, A. Erdem, S.-k. Hu, M.R. Dokmeci, A.S. Nasr, A. Khademhosseini, Advances in controlled oxygen generating biomaterials for tissue engineering and regenerative therapy, Biomacromolecules, 21 (2019) 56-72.

[3] S. Moghassemi, A. Dadashzadeh, R.B. Azevedo, C.A. Amorim, Nanoemulsion applications in photodynamic therapy, Journal of Controlled Release, 351 (2022) 164-173.

[4] S. Suvarnapathaki, X. Wu, D. Lantigua, M.A. Nguyen, G. Camci-Unal, Breathing life into engineered tissues using oxygen-releasing biomaterials, NPG Asia Materials, 11 (2019) 1-18.

[5] M. Gholipourmalekabadi, S. Zhao, B.S. Harrison, M. Mozafari, A.M. Seifalian, Oxygen-generating biomaterials: a new, viable paradigm for tissue engineering?, Trends in biotechnology, 34 (2016) 1010-1021.

[6] S.I.H. Abdi, S.M. Ng, J.O. Lim, An enzyme-modulated oxygen-producing micro-system for regenerative therapeutics, International journal of pharmaceutics, 409 (2011) 203-205.

[7] S.I.H. Abdi, J.Y. Choi, H.C. Lau, J.O. Lim, Controlled release of oxygen from PLGA-alginate layered matrix and its in vitro characterization on the viability of muscle cells under hypoxic environment, Tissue Engineering and Regenerative Medicine, 10 (2013) 131-138.
[8] Z. Li, X. Guo, J. Guan, An oxygen release system to augment cardiac progenitor cell survival and differentiation under hypoxic condition, Biomaterials, 33 (2012) 5914-5923.
[9] C.R. Gordijo, A.Z. Abbasi, M.A. Amini, H.Y. Lip, A. Maeda, P. Cai, P.J. O'Brien, R.S. DaCosta, A.M. Rauth, X.Y. Wu, Design of Hybrid MnO2-Polymer-Lipid Nanoparticles with Tunable Oxygen Generation Rates and Tumor Accumulation for Cancer Treatment, Advanced Functional Materials, 25 (2015) 1858-1872.
[10] G. Song, Y. Chen, C. Liang, X. Yi, J. Liu, X. Sun, S. Shen, K. Yang, Z. Liu, Catalase-loaded TaOx nanoshells as bio-nanoreactors combining high-Z element and enzyme delivery for enhancing radiotherapy, Advanced materials, 28 (2016) 7143-7148.
[11] B.J. Buckley, A.K. Tanswell, B.A. Freeman, Liposome-mediated augmentation of catalase in alveolar type II cells protects against H2O2 injury, Journal of Applied Physiology, 63 (1987) 359-367.
[12] A.A. Frimer, A. Forman, D.C. Borg, H2O2-diffusion through liposomes, Israel Journal of Chemistry, 23 (1983) 442-445.
[13] X. Song, J. Xu, C. Liang, Y. Chao, Q. Jin, C. Wang, M. Chen, Z. Liu, Self-supplied tumor oxygenation through separated liposomal delivery of H2O2 and catalase for enhanced radio-immunotherapy of cancer, Nano letters, 18 (2018) 6360-6368.
[14] H. Jafari, A. Dadashzadeh, S. Moghassemi, P. Zahedi, C.A. Amorim, A. Shavandi, Ovarian cell encapsulation in an enzymatically crosslinked silk-based hydrogel with tunable mechanical properties, Gels, 7 (2021) 138.
[15] H. Jafari, H. Alimoradi, C. Delporte, K.V. Bernaerts, R. Heidari, D. Podstawczyk, S.V. Niknezhad, A. Shavandi, An injectable, self-healing, 3D printable, double network co-enzymatically crosslinked hydrogel using marine poly-and oligo-saccharides for wound healing application, Applied Materials Today, 29 (2022) 101581.
[16] M. Khanmohammadi, M.B. Dastjerdi, A. Ai, A. Ahmadi, A. Godarzi, A. Rahimi, J. Ai, Horseradish peroxidase-catalyzed hydrogelation for biomedical applications, Biomaterials science, 6 (2018) 1286-1298.
[17] K.M. Park, Y. Lee, J.Y. Son, J.W. Bae, K.D. Park, In situ SVVYGLR peptide conjugation into injectable gelatin-poly (ethylene glycol)-tyramine hydrogel via enzyme-mediated reaction for enhancement of endothelial cell activity and neo-vascularization, Bioconjugate chemistry, 23 (2012) 2042-2050.
[18] R. Wang, X. Huang, B. Zoetebier, P.J. Dijkstra, M. Karperien, Enzymatic co-crosslinking of star-shaped poly (ethylene glycol) tyramine and hyaluronic acid tyramine conjugates provides elastic biocompatible and biodegradable hydrogels, Bioactive Materials, 20 (2023) 53-63.
[19] Y. Liu, S. Sakai, M. Taya, Impact of the composition of alginate and gelatin derivatives in bioconjugated hydrogels on the fabrication of cell sheets and spherical tissues with living cell sheaths, Acta biomaterialia, 9 (2013) 6616-6623.
[20] P. Yingyuad, C. Sinthuvanich, T. Leepasert, P. Thongyoo, S. Boonrungsiman, Preparation, characterization and in vitro evaluation of calothrixin B liposomes, Journal of drug delivery science and technology, 44 (2018) 491-497.

[21] D.L. Tran, P. Le Thi, T.T.H. Thi, K.D. Park, Novel enzymatically crosslinked chitosan hydrogels with free-radical-scavenging property and promoted cellular behaviors under hyperglycemia, Progress in Natural Science: Materials International, 30 (2020) 661-668.
[22] K. Ren, B. Li, Q. Xu, C. Xiao, C. He, G. Li, X. Chen, Enzymatically crosslinked hydrogels based on linear poly (ethylene glycol) polymer: performance and mechanism, Polymer Chemistry, 8 (2017) 7017-7024.
[23] S. Moghassemi, E. Parnian, A. Hakamivala, M. Darzianiazizi, M.M. Vardanjani, S. Kashanian, B. Larijani, K. Omidfar, Uptake and transport of insulin across intestinal membrane model using trimethyl chitosan coated insulin niosomes, Materials science and engineering: C, 46 (2015) 333-340.
[24] K.H. Fisher-Wellman, L.A. Gilliam, C.-T. Lin, B.L. Cathey, D.S. Lark, P.D. Neufer, Mitochondrial glutathione depletion reveals a novel role for the pyruvate dehydrogenase complex as a key H2O2-emitting source under conditions of nutrient overload, Free Radical Biology and Medicine, 65 (2013) 1201-1208.
[25] T. Komlódi, O. Sobotka, E. Gnaiger, Facts and artefacts on the oxygen dependence of hydrogen peroxide flux using Amplex UltraRed, Bioenergetics Communications, 2021 (2021) 4-4.
[26] M. Zhang, T. Kiratiwongwan, W. Shen, Oxygen-releasing polycaprolactone/calcium peroxide composite microspheres, Journal of Biomedical Materials Research Part B: Applied Biomaterials, 108 (2020) 1097-1106.
[27] P. Ghaffari-Bohlouli, H. Alimoradi, D.F.S. Petri, S. Moghassemi, C.A. Amorim, L. Nie, A. Shavandi, Alleviating hypoxia through self-generating oxygen and hydrogen peroxide fluorinated chitosan: Insights from a kinetic study, Chemical Engineering Journal, (2023) 145072.
[28] T. Li, X. Song, C. Weng, X. Wang, J. Wu, L. Sun, X. Gong, W.-N. Zeng, L. Yang, C. Chen, Enzymatically crosslinked and mechanically tunable silk fibroin/pullulan hydrogels for mesenchymal stem cells delivery, International journal of biological macromolecules, 115 (2018) 300-307.
[29] H. Jafari, P. Ghaffari-Bohlouli, D. Podstawczyk, L. Nie, A. Shavandi, Tannic acid post-treatment of enzymatically crosslinked chitosan-alginate hydrogels for biomedical applications, Carbohydrate Polymers, 295 (2022) 119844.
[30] J. Vanacker, V. Luyckx, M.-M. Dolmans, A. Des Rieux, J. Jaeger, A. Van Langendonckt, J. Donnez, C.A. Amorim, Transplantation of an alginate–matrigel matrix containing isolated ovarian cells: first step in developing a biodegradable scaffold to transplant isolated preantral follicles and ovarian cells, Biomaterials, 33 (2012) 6079-6085.
[31] A. Dadashzadeh, S. Moghassemi, C. Amorim, Evaluation of PEGylated fibrin as a three-dimensional biodegradable scaffold for ovarian tissue engineering, Materials Today Chemistry, 22 (2021) 100626.
[32] A. Dadashzadeh, S. Moghassemi, M. Grubliauskaité, H. Vlieghe, D. Brusa, C.A. Amorim, Medium supplementation can influence the human ovarian cells in vitro, Journal of ovarian research, 15 (2022) 1-12.
[33] A. Dadashzadeh, S. Moghassemi, A. Peaucelle, C.M. Lucci, C.A. Amorim, Mind the mechanical strength: tailoring a 3D matrix to encapsulate isolated human preantral follicles, Human Reproduction Open, 2023 (2023) hoad004.

[34] S. Moghassemi, A. Dadashzadeh, A. Camboni, O. Feron, R.B. Azevedo, C.A. Amorim, Photodynamic therapy using OR141-loaded nanovesicles for eradication of leukemic cells from ovarian tissue, Photodiagnosis and photodynamic therapy, 40 (2022) 103139.
[35] E.A. Jaimes, C. Sweeney, L. Raij, Effects of the reactive oxygen species hydrogen peroxide and hypochlorite on endothelial nitric oxide production, Hypertension, 38 (2001) 877-883.
[36] I.U. Schraufstatter, D.B. Hinshaw, P.A. Hyslop, R.G. Spragg, C.G. Cochrane, Oxidant injury of cells. DNA strand-breaks activate polyadenosine diphosphate-ribose polymerase and lead to depletion of nicotinamide adenine dinucleotide, The Journal of clinical investigation, 77 (1986) 1312-1320.
[37] J. Harlan, J. Levine, K. Callahan, B. Schwartz, L. Harker, Glutathione redox cycle protects cultured endothelial cells against lysis by extracellularly generated hydrogen peroxide, The Journal of clinical investigation, 73 (1984) 706-713.
[38] S. Moghassemi, A. Dadashzadeh, A. Camboni, O. Feron, R.B. Azevedo, C.A. Amorim, Ex vivo purging of cancer cells from ovarian tissue using photodynamic therapy: a novel strategy to restore fertility in leukemia patients, Human Reproduction Open, 2023 (2023) hoad005.
[39] S. Moghassemi, A. Dadashzadeh, P.E.N. de Souza, R.B. Azevedo, C.A. Amorim, AlPc/ZnPc-based oncological photodynamic therapy for a selective eradication of leukemic cells from ovarian tissue, Photodiagnosis and photodynamic therapy, 36 (2021) 102555.
[40] S. Bhattacharjee, DLS and zeta potential–what they are and what they are not?, Journal of controlled release, 235 (2016) 337-351.
[41] P. Singh, J. Bodycomb, B. Travers, K. Tatarkiewicz, S. Travers, G.R. Matyas, Z. Beck, Particle size analyses of polydisperse liposome formulations with a novel multispectral advanced nanoparticle tracking technology, International journal of pharmaceutics, 566 (2019) 680-686.
[42] M. Danaei, M. Dehghankhold, S. Ataei, F. Hasanzadeh Davarani, R. Javanmard, A. Dokhani, S. Khorasani, M. Mozafari, Impact of particle size and polydispersity index on the clinical applications of lipidic nanocarrier systems, Pharmaceutics, 10 (2018) 57.
[43] V.R. Patel, Y. Agrawal, Nanosuspension: An approach to enhance solubility of drugs, Journal of advanced pharmaceutical technology & research, 2 (2011) 81.
[44] M. Yoshimoto, H. Sakamoto, N. Yoshimoto, R. Kuboi, K. Nakao, Stabilization of quaternary structure and activity of bovine liver catalase through encapsulation in liposomes, Enzyme and microbial technology, 41 (2007) 849-858.
[45] K. Ullmann, G. Leneweit, H. Nirschl, How to achieve high encapsulation efficiencies for macromolecular and sensitive APIs in liposomes, Pharmaceutics, 13 (2021) 691.
[46] D. Guo, J. Liu, Y. Fan, J. Cheng, Y. Shi, J. Zou, X. Zhang, Optimization, characterization and evaluation of liposomes from Malus hupehensis (Pamp.) Rehd. extracts, Journal of liposome research, 30 (2020) 366-376.
[47] L. Shi, J. Zhang, M. Zhao, S. Tang, X. Cheng, W. Zhang, W. Li, X. Liu, H. Peng, Q. Wang, Effects of polyethylene glycol on the surface of nanoparticles for targeted drug delivery, Nanoscale, 13 (2021) 10748-10764.
[48] T.T. Hoang Thi, Y. Lee, P. Le Thi, K.D. Park, Oxidized alginate supplemented gelatin hydrogels for the in situ formation of wound dressing with high antibacterial activity, Macromolecular Research, 27 (2019) 811-820.
[49] S.D. Kim, S. Jin, S. Kim, D. Son, M. Shin, Tyramine-Functionalized Alginate-Collagen Hybrid Hydrogel Inks for 3D-Bioprinting, Polymers, 14 (2022) 3173.

[50] S. Sakai, M. Nakahata, Horseradish peroxidase catalyzed hydrogelation for biomedical, biopharmaceutical, and biofabrication applications, Chemistry–An Asian Journal, 12 (2017) 3098-3109.
[51] P. Le Thi, Y. Lee, D.L. Tran, T.T.H. Thi, K.M. Park, K.D. Park, Calcium peroxide-mediated in situ formation of multifunctional hydrogels with enhanced mesenchymal stem cell behaviors and antibacterial properties, Journal of Materials Chemistry B, 8 (2020) 11033-11043.
[52] H.S. Samanta, S.K. Ray, Synthesis, characterization, swelling and drug release behavior of semi-interpenetrating network hydrogels of sodium alginate and polyacrylamide, Carbohydrate polymers, 99 (2014) 666-678.
[53] H. Jafari, C. Delporte, K.V. Bernaerts, H. Alimoradi, L. Nie, D. Podstawczyk, K.C. Tam, A. Shavandi, Synergistic complexation of phenol functionalized polymer induced in situ microfiber formation for 3D printing of marine-based hydrogels, Green Chemistry, 24 (2022) 2409-2422.
[54] C. Qiao, G. Chen, J. Zhang, J. Yao, Structure and rheological properties of cellulose nanocrystals suspension, Food Hydrocolloids, 55 (2016) 19-25.
[55] J. Liu, B. Yang, M. Li, J. Li, Y. Wan, Enhanced dual network hydrogels consisting of thiolated chitosan and silk fibroin for cartilage tissue engineering, Carbohydrate polymers, 227 (2020) 115335.
[56] W. Wu, Y. Dai, H. Liu, R. Cheng, Q. Ni, T. Ye, W. Cui, Local release of gemcitabine via in situ UV-crosslinked lipid-strengthened hydrogel for inhibiting osteosarcoma, Drug Delivery, 25 (2018) 1642-1651.
[57] K. Elkhoury, L. Sanchez-Gonzalez, P. Lavrador, R. Almeida, V. Gaspar, C. Kahn, F. Cleymand, E. Arab-Tehrany, J.F. Mano, Gelatin methacryloyl (GelMA) nanocomposite hydrogels embedding bioactive naringin liposomes, Polymers, 12 (2020) 2944.
[58] G. Camci-Unal, N. Alemdar, N. Annabi, A. Khademhosseini, Oxygen-releasing biomaterials for tissue engineering, Polymer international, 62 (2013) 843-848.
[59] A.L. Farris, A.N. Rindone, W.L. Grayson, Oxygen delivering biomaterials for tissue engineering, Journal of materials chemistry B, 4 (2016) 3422-3432.
[60] S. Moghassemi, A. Dadashzadeh, R.B. de Azevedo, C.A. Amorim, Secure transplantation by tissue purging using photodynamic therapy to eradicate malignant cells, Journal of Photochemistry and Photobiology B: Biology, (2022) 112546.
[61] C.L. Ward, B.T. Corona, J.J. Yoo, B.S. Harrison, G.J. Christ, Oxygen generating biomaterials preserve skeletal muscle homeostasis under hypoxic and ischemic conditions, PloS one, 8 (2013) e72485.